Signal Processing 89 (2009) 1403–1411

Contents lists available at ScienceDirect

Signal Processing

journal homepage: www.elsevier.com/locate/sigpro

Conjugate unitary ESPRIT for real sources adapted to the coherent case ☆

Zhigang Liu *, Jinkuan Wang, Fuli Wang

School of Information Science and Engineering, Northeastern University, Shenyang, China

ARTICLE INFO

Article history:
Received 17 May 2007
Received in revised form
6 January 2009
Accepted 13 January 2009
Available online 8 February 2009

Keywords:
Array signal processing
Direction-of-arrival (DOA)
NC unitary ESPRIT
ESPRIT

ABSTRACT

By virtue of real-valued property of some real sources, in this paper, we suggest a conjugate unitary ESPRIT (CU-ESPRIT) algorithm to exploit the conjugate information of partial array element outputs. To deal with correlated or coherent sources, we design a virtual centro-symmetric array and divide it into the virtual subarrays. Compared with the unitary ESPRIT for non-circular sources (NC unitary ESPRIT), CU-ESPRIT achieves a relative reduction of the computational complexity and an improved resolution for uncorrelated or coherent sources. Specifically, this algorithm can estimate as many as $M-1$ coherent sources for an array of M elements. Simulation results show the validity of our approach.

1. Introduction

The problem of reducing the computational complexity of eigenspace-based methods via real-valued decomposition has recently drawn considerable attentions (see literatures [1–6] and the references therein). For an array of centro-symmetric configurations, Haardt and Nossek developed the unitary ESPRIT algorithm by incorporating forward–backward averaging [3]. Pesavento et al. further studied the centro-Hermitian property of the forward–backward spatial smoothing autocorrelation matrix, and proposed the unitary root-MUSIC algorithm with real-valued eigendecomposition for partially correlated or coherent sources [6].

As we know that in many modern telecommunication systems or satellite systems, some non-circular sources like MASK, AM, or BPSK modulated signals are of real value. After studying the real-valued property, Tayem brought forward the conjugate ESPRIT algorithm [7]. In this approach, the array elements are divided into two subarrays. By adding the conjugate information of some array element output, this algorithm can estimate a maximum of M uncorrelated real-valued signals, which equals to the total number of array elements. To utilize the conjugate information of all the element outputs, the unitary ESPRIT for non-circular sources (NC unitary ESPRIT) is proposed in [8,9]. NC unitary ESPRIT virtually doubles the number of antennas and so as to achieve a better performance for coherent signals in contrast to unitary ESPRIT.

In this paper, we propose to exploit the conjugate information of partial array element outputs by designing a virtual centro-symmetric array for the factual uniform linear array (ULA). The new approach, named as conjugate unitary ESPRIT (CU-ESPRIT), has a reduced computational complexity and improved resolution in comparison with NC unitary ESPRIT. Specifically, since we divide the virtual centro-symmetric array of $2M-1$ virtual sensors into M overlapping subarrays of size M like spatial smoothing techniques [10–12], we can estimate up to $M-1$ coherent real-valued signals.

☆ This work was supported by the doctor foundation from the Ministry of Education of China, under Grant no. 20050145019.

* Corresponding author.
E-mail address: zliu@mail.neuq.edu.cn (Z. Liu).

0165-1684/$ - see front matter © 2009 Elsevier B.V. All rights reserved.
doi:10.1016/j.sigpro.2009.01.011

The rest of the paper is organized as follows. In the next section, we briefly present the signal model of the ULA. In Section 3, we give how to design the virtual centro-symmetric array and the derivation of CU-ESPRIT for uncorrelated signals. Similarly, Section 4 designs the special virtual subarrays and the formulation of CU-ESPRIT for coherent signals. Section 5 provides the performance analysis of this proposed algorithm from the maximum number of estimated coherent signals and the elapsed CPU time in contrast with classical ESPRIT [13] and NC unitary ESPRIT. Section 6 gives several simulation results that compare our approach with ESPRIT and NC unitary ESPRIT, and the paper concludes in Section 7.

2. Signal model

Consider a ULA with M omnidirectional sensors, suppose d narrowband far-field signals impinging from the directions $\theta_1,\ldots,\theta_d$, and assume that the non-circular sources are real-valued at the receiver for all the stationary users. In order to make these non-circular sources real-valued at the receiver, the transmit delays of all the users must be preestimated by MUSIC or ESPRIT, and compensated in practical systems, e.g. mobile systems.

When the superscript T denotes the transpose of a vector or matrix, the $M\times 1$ array observation vector $[x_1(t),x_2(t),\ldots,x_M(t)]^T$ is modelled as

$$\mathbf{x}(t)=\sum_{i=1}^{d}\mathbf{a}(\theta_i)s_i(t)\exp(j\phi_i)+\mathbf{n}(t) \tag{1}$$

where $s_i(t)$ represents the signal from the ith sources with direction-of-arrival (DOA) θ_i, $\mathbf{n}(t)$ is the $M\times 1$ vector of additive white Gaussian noises (AWGNs) with each component of mean zero and variance σ^2, and the factor $\exp(j\phi_i)$ denotes arbitrary complex phase shift for the ith source due to the transmit delays. Since this factor can make these non-circular sources complex-valued at the receiver, it should be estimated by MUSIC or ESPRIT and compensated, that is, $\phi_i\approx 0$.

The $M\times 1$ array steering vector can be written as

$$\mathbf{a}(\theta_i)=[1,z_i,z_i^2,\ldots,z_i^{M-1}]^T,\quad i=1,\ldots,d \tag{2}$$

where $z_i=\exp(-j2\pi\Delta\sin\theta_i/\lambda)$, λ is the wavelength, and Δ denotes the spacing between two successive array elements. The $M\times d$ array response matrix and $d\times 1$ signal vector can be written as

$$\mathbf{A}=[\mathbf{a}(\theta_1),\mathbf{a}(\theta_2),\ldots,\mathbf{a}(\theta_d)] \tag{3}$$

and

$$\mathbf{s}(t)=[s_1(t),s_2(t),\ldots,s_d(t)]^T \tag{4}$$

respectively. To further simplify the notation, we rewrite (1) as

$$\mathbf{x}(t)=\mathbf{A}\mathbf{s}(t)+\mathbf{n}(t) \tag{5}$$

Finally, the covariance matrix of the array observation vector can be defined by

$$\mathbf{R}=E\{\mathbf{x}(t)\mathbf{x}^H(t)\}=\mathbf{A}\mathbf{S}\mathbf{A}^H+\sigma^2\mathbf{I}_M \tag{6}$$

where

$$\mathbf{S}=E\{\mathbf{s}(t)\mathbf{s}^H(t)\} \tag{7}$$

is the $d\times d$ signal covariance matrix, $\mathbf{I}_M$ is the $M\times M$ identity matrix, and the superscript H stands for the complex conjugate transpose of a vector or matrix.

3. Uncorrelated signals

3.1. Virtual centro-symmetric array

Making use of the real-valued property of non-circular sources, the CU-ESPRIT takes sample data from all the elements and their conjugate information, and arranges them in a column vector $[x_M^*(t),\ldots,x_2^*(t),x_1(t),x_2(t),\ldots,x_M(t)]^T$, where the superscript $*$ denotes the conjugate. The column vector is used for the virtual array processing. Therefore, the designed array corresponding to this vector is called as the virtual array in Fig. 1, which has $2M-1$ virtual array elements in all. In contrast with the factual array, the virtual array increases the number of array elements, and this transforms the signal model of the factual array.

Let the first element of the factual array be the reference with respect to the other elements. For the uncorrelated real signals where $s_i(t)=s_i^*(t)$, the $(2M-1)\times 1$ observation vector of the virtual array can be defined as

$$\mathbf{X}(t)=[x_M^*(t),\ldots,x_2^*(t),x_1(t),x_2(t),\ldots,x_M(t)]^T \tag{8}$$

or

$$\mathbf{X}(t)=\begin{pmatrix}\sum_{i=1}^{d}s_i(t)z_i^{*(M-1)}+n_M^*(t)\\ \vdots\\ \sum_{i=1}^{d}s_i(t)z_i^{*}+n_2^*(t)\\ \sum_{i=1}^{d}s_i(t)+n_1(t)\\ \sum_{i=1}^{d}s_i(t)z_i+n_2(t)\\ \vdots\\ \sum_{i=1}^{d}s_i(t)z_i^{M-1}+n_M(t)\end{pmatrix} \tag{9}$$

Using (8) and (9), we can rewrite (5) as

$$\mathbf{X}(t)=\mathbf{A}_v\mathbf{s}(t)+\mathbf{N}(t) \tag{10}$$

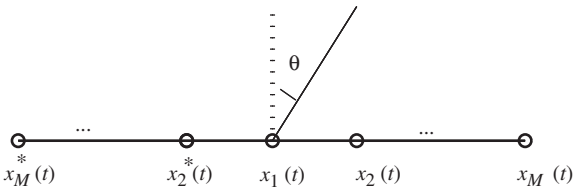

Fig. 1. The virtual centro-symmetric array consisting of a column vector $[x_M^*(t),\ldots,x_2^*(t),x_1(t),x_2(t),\ldots,x_M(t)]^T$.

where $\mathbf{A}_v$ is the $(2M-1)\times d$ response matrix of the virtual array

$$\mathbf{A}_v=[\mathbf{a}_v(\theta_1),\mathbf{a}_v(\theta_2),\ldots,\mathbf{a}_v(\theta_d)] \tag{11}$$

and the $(2M-1)\times 1$ steering vector of the virtual array can be written as

$$\mathbf{a}_v(\theta_i)=[z_i^{-(M-1)},\ldots,z_i^{-1},1,z_i,\ldots,z_i^{M-1}]^T,\quad i=1,\ldots,d \tag{12}$$

and the $(2M-1)\times 1$ AWGN vector of the virtual array can be given as

$$\mathbf{N}(t)=[n_{M-1}^*(t),\ldots,n_2^*(t),n_1(t),n_2(t),\ldots,n_{M-1}(t)]^T \tag{13}$$

From Eq. (12), we can draw the important conclusions that the virtual array manifold is conjugate centro-symmetric when employing the center of the virtual ULA as the phase reference, and that the number of all the elements comprising the virtual ULA is odd.

3.2. Real-valued decomposition

First of all, let us introduce our notation and review the definition of centro-Hermitian matrices. Suppose that $\mathbf{J}_m\in C^{m\times m}$ is the exchange matrix with ones on its antidiagonal and zeros elsewhere, and with this notation, we can define centro-Hermitian matrices.

Definition 1. A complex matrix $\mathbf{M}\in C^{m\times m}$ is called centro-Hermitian if

$$\mathbf{J}_m\mathbf{M}^*\mathbf{J}_m=\mathbf{M}$$

Based on this definition, we will prove the important property of the designed virtual array.

Theorem 1. *The covariance matrix $\mathbf{R}_v$ of the virtual array is centro-Hermitian.*

Proof. For the virtual array manifold is conjugate centro-symmetric, we can get the first important equation as follows:

$$\mathbf{J}_{2M-1}\mathbf{A}_v^*=\mathbf{A}_v \tag{14}$$

and for non-circular sources have real-valued property, we can obtain the second important equation about the signal covariance matrix as follows:

$$\mathbf{S}^*=\mathbf{S} \tag{15}$$

Using Eq. (6), the covariance matrix of the virtual array can be defined by

$$\mathbf{R}_v=E\{\mathbf{X}(t)\mathbf{X}^H(t)\}=\mathbf{A}_v\mathbf{S}\mathbf{A}_v^H+\sigma^2\mathbf{I}_{2M-1} \tag{16}$$

Using Eqs. (14) and (15), and by multiplying the complex conjugation form of the covariance matrix of the virtual array on both sides with the exchange matrix $\mathbf{J}$, we can obtain a matrix in the following fashion:

$$\begin{aligned}\mathbf{J}_{2M-1}\mathbf{R}_v^*\mathbf{J}_{2M-1}&=\mathbf{J}_{2M-1}\mathbf{A}_v^*\mathbf{S}^*[\mathbf{A}_v^*]^H\mathbf{J}_{2M-1}+\sigma^2\mathbf{I}_{2M-1}\\&=\mathbf{A}_v\mathbf{S}^*\mathbf{A}_v^H+\sigma^2\mathbf{I}_{2M-1}\\&=\mathbf{R}_v\end{aligned} \tag{17}$$

Finally, from Definition 1, we can conclude that the covariance matrix $\mathbf{R}_v$ of the virtual array has centro-Hermitian property.

By exploiting the centro-Hermitian property of the covariance matrix $\mathbf{R}_v$ of the virtual array, we derive the real-valued matrix as

$$\mathbf{C}_v=\mathbf{Q}_{2M-1}^H\mathbf{R}_v\mathbf{Q}_{2M-1} \tag{18}$$

where $\mathbf{Q}_n$ is any unitary column conjugate symmetric matrix, for example

$$\mathbf{Q}_{2n}=\frac{1}{\sqrt{2}}\begin{bmatrix}\mathbf{I}_n & j\mathbf{I}_n\\ \mathbf{J}_n & -j\mathbf{J}_n\end{bmatrix}$$

and

$$\mathbf{Q}_{2n+1}=\frac{1}{\sqrt{2}}\begin{bmatrix}\mathbf{I}_n & \mathbf{0}_{n\times 1} & j\mathbf{I}_n\\ \mathbf{0}_{n\times 1}^T & \sqrt{2} & \mathbf{0}_{n\times 1}^T\\ \mathbf{J}_n & \mathbf{0}_{n\times 1} & -j\mathbf{J}_n\end{bmatrix}$$

can be chosen for arrays with an even and odd number of sensors, respectively, where $\mathbf{0}_{n\times 1}$ is the $n\times 1$ matrix of zeros. Note that the number of the virtual ULA is odd, we only choose the latter. Then four properties of this matrix $\mathbf{Q}_n$ are displayed as follows:

$$\mathbf{Q}_{2n}^H\mathbf{a}_v=\mathbf{b}_v \tag{19}$$

with $\mathbf{a}_v=[\mathbf{a}^T,(\mathbf{J}_n\mathbf{a}^*)^T]^T$ and $\mathbf{b}_v=[\mathrm{Re}(\mathbf{a}^T),\mathrm{Im}(\mathbf{a}^T)]^T$.

$$\mathbf{Q}_{2n}^H\mathbf{a}_v\exp(jw)=\mathbf{b}_{v1} \tag{20}$$

where $\mathrm{Re}(\mathbf{b}_{v1})=\mathbf{b}_v\cos(w)$ and $\mathrm{Im}(\mathbf{b}_{v1})=\mathbf{b}_v\sin(w)$.

$$\mathbf{Q}_{2n+1}^H\mathbf{a}_{v2}=\mathbf{b}_{v2} \tag{21}$$

with $\mathbf{a}_{v2}=[\mathbf{a}^T,1,(\mathbf{J}_n\mathbf{a}^*)^T]^T$ and $\mathbf{b}_{v2}=[\mathrm{Re}(\mathbf{a}^T),1,\mathrm{Im}(\mathbf{a}^T)]^T$.

$$\mathbf{Q}_n\mathbf{Q}_n^H=\mathbf{I}_n \tag{22}$$

Below these properties, Eq. (18) may be rewritten as

$$\mathbf{C}_v=\mathbf{B}_v\mathbf{S}\mathbf{B}_v^H+\sigma^2\mathbf{I}_{2M-1} \tag{23}$$

where $\mathbf{B}_v=[\mathrm{Re}(\mathbf{A}^T),\mathbf{1}_{1\times d}^T,\mathrm{Im}(\mathbf{A}^T)]^T$, and $\mathbf{1}_{1\times d}$ is the $1\times d$ matrix of ones. Correspondingly $\mathbf{A}_v=[\mathbf{A}^T,\mathbf{1}_{1\times d}^T,(\mathbf{J}_n\mathbf{A}^*)^T]^T$ in Eq. (16).

In the way the expression of the signal subspace $\mathbf{E}_s$ is $\mathbf{E}_s=\mathbf{B}_v\mathbf{T}$ with T a real matrix. As $\mathbf{B}_v=\mathbf{Q}_{2M-1}^H\mathbf{A}_v$, then $\mathbf{Q}_{2M-1}\mathbf{E}_s=\mathbf{A}_v\mathbf{T}$ from Eq. (22). As $\mathbf{J}_v$ is the special matrix $[\mathbf{0}_{(2M-2)\times 1},\mathbf{I}_{2M-2}]$, then

$$\mathbf{J}_v\mathbf{Q}_{2M-1}\mathbf{E}_s=\mathbf{J}_v\mathbf{A}_v\mathbf{T}$$

As $\mathbf{J}_v\mathbf{A}_v=\mathbf{A}_0\mathbf{\Phi}$ with $\mathbf{\Phi}=\mathrm{diag}\{z_1,\ldots,z_d\}$, then

$$\mathbf{Q}_{2M-2}^H\mathbf{J}_v\mathbf{Q}_{2M-1}\mathbf{E}_s=\mathbf{B}_0\mathbf{\Phi}\mathbf{T} \tag{24}$$

with $\mathbf{B}_0=[\mathrm{Re}(\mathbf{A}_0^T),\mathrm{Im}(\mathbf{A}_0^T)]^T$ from Eq. (19). As $\mathbf{B}_0$, $\mathbf{E}_s$ and $\mathbf{T}$ are real, then

$$\mathbf{K}_{v1}\mathbf{E}_s=\mathbf{B}_0\cos(\mathbf{\Phi})\mathbf{T}=\mathbf{E}_{s1} \tag{25}$$

with

$$\mathbf{K}_{v1}=\mathrm{Re}\{\mathbf{Q}_{2M-2}^H\mathbf{J}_v\mathbf{Q}_{2M-1}\}$$

and

$$\mathbf{K}_{v2}\mathbf{E}_s=\mathbf{B}_0\sin(\mathbf{\Phi})\mathbf{T}=\mathbf{E}_{s2} \tag{26}$$

with

$$\mathbf{K}_{v2} = \mathrm{Im}\{\mathbf{Q}_{2M-2}^H \mathbf{J}_v \mathbf{Q}_{2M-1}\}$$

Therefore, the important matrix equation [4] is given as

$$\mathbf{K}_{v1}\mathbf{E}_s\boldsymbol{\Psi} = \mathbf{K}_{v2}\mathbf{E}_s \tag{27}$$

where

$$\boldsymbol{\Psi} = \mathbf{T}^{-1}\boldsymbol{\Phi}_0\mathbf{T}$$

and

$$\boldsymbol{\Phi}_0 = \frac{\sin(\boldsymbol{\Phi})}{\cos(\boldsymbol{\Phi})} = \mathrm{diag}\{w_1,\ldots,w_d\}$$

with

$$w_i = \frac{Im(z_i)}{Re(z_i)} = \tan\left(-\frac{\pi\Delta\sin(\theta_i)}{\lambda}\right).$$

In practice, the estimate of the covariance matrix $\mathbf{R}_v$ of the virtual array is given by

$$\hat{\mathbf{R}}_v = \frac{1}{N}\sum_{k=1}^{N}\mathbf{X}(k)\mathbf{X}^H(k)$$

where N denotes the number of the snapshots. Due to a residual imaginary part from the noise covariance, $\hat{\mathbf{R}}_v$ is not exactly centro-Hermitian. To avoid this residual imaginary part, Eq. (18) is rewritten as follows:

$$\hat{\mathbf{C}}_v = \mathrm{Re}\{\mathbf{Q}_{2M-1}^H\hat{\mathbf{R}}_v\mathbf{Q}_{2M-1}\} \tag{28}$$

3.3. Summary

For uncorrelated sources, the procedure of CU-ESPRIT is summarized in the following.

Algorithm 1.

Step 1. Form the observation vector of the virtual array and the real-valued matrix $\hat{\mathbf{C}}_v$.
Step 2. Find the signal subspace $\mathbf{E}_s$ by taking EVD of the matrix $\hat{\mathbf{C}}_v$.
Step 3. Compute $\boldsymbol{\Psi}$ as the solution to the matrix equation $(\mathbf{K}_{v1}\mathbf{E}_s)\boldsymbol{\Psi} = (\mathbf{K}_{v2}\mathbf{E}_s)$.
Step 4. Compute $\omega_i, i = 1,\ldots,d$ as the eigenvalues of the $d\times d$ real-valued matrix $\boldsymbol{\Psi}$.
Step 5. Estimate DOAs of signals of interest (SOI) from

$$\theta_k = \arcsin\left(-\frac{\lambda}{\pi\Delta}\arctan\omega_k\right), \quad k = 1,\ldots,d \tag{29}$$

4. Coherent signals

4.1. Virtual subarrays

To separate highly correlated or coherent real sources, virtual subarrays are proposed like Shan's spatial smoothing method. This approach is a preprocessing scheme which divides the virtual centro-symmetric array of $2M-1$ virtual sensors into M overlapping backward subarrays of size M, with virtual sensors $[x_1(t),x_2(t),x_3(t),\ldots,x_M(t)]^T$ forming the first virtual subarray, virtual sensors $[x_2^*(t),x_1(t),x_2(t),\ldots,x_{M-1}(t)]^T$ forming the second virtual subarray, virtual sensors $[x_3^*(t),x_2^*(t),x_1(t),\ldots,x_{M-2}(t)]^T$ forming the third virtual subarray, etc. Therefore, the vector of received signals at the kth virtual subarray can be written as

$$\mathbf{x}_k(t) = \mathbf{A}\boldsymbol{\Phi}^{*(k-1)}\mathbf{s}(t) + \mathbf{n}_k(t) \tag{30}$$

where $\boldsymbol{\Phi}^*$ denotes the conjugation of the $d\times d$ invariant matrix

$$\boldsymbol{\Phi}^* = \mathrm{diag}\{e^{j(2\pi/\lambda)\Delta\sin\theta_1}, e^{j(2\pi/\lambda)\Delta\sin\theta_2},\ldots,e^{j(2\pi/\lambda)\Delta\sin\theta_d}\}$$

and the covariance matrix of the kth virtual subarray is given by

$$\mathbf{R}_k = \mathbf{A}\boldsymbol{\Phi}^{*(k-1)}\mathbf{S}[\boldsymbol{\Phi}^{*(k-1)}]^H\mathbf{A}^H + \sigma^2\mathbf{I}_M \tag{31}$$

Thus, the spatial smoothing covariance matrix can be defined as the sample mean of the virtual subarray covariances

$$\mathbf{R}_s = \frac{1}{M}\sum_{k=1}^{M}\mathbf{R}_k \tag{32}$$

Using (31), Eq. (32) can be compactly rewritten as

$$\mathbf{R}_s = \mathbf{A}\mathbf{S}_s\mathbf{A}^H + \sigma^2\mathbf{I}_M \tag{33}$$

where $\mathbf{S}_s$ is the modified virtual covariance of the signals, given by

$$\mathbf{S}_s = \frac{1}{M}\sum_{k=1}^{M}\boldsymbol{\Phi}^{*(k-1)}\mathbf{S}[\boldsymbol{\Phi}^{*(k-1)}]^H \tag{34}$$

In [10], it was proven that the modified covariance matrix of signals is nonsingular if the number of subarrays is greater than or equal to the number of signals. Then the important theorem can be obtained as

Theorem 2. *If the number of subarrays M is greater than the number of signals d,* i.e., *if $M>d$, the modified virtual covariance of the signals is nonsingular.*

Note that this approach must limit spatial smoothing technique to M virtual subarrays of size M, and can estimate up to $M-1$ coherent sources without a reduced effective aperture, because the maximum number of estimated sources should be smaller than the size of the subarrays. Similar to the real-valued covariance matrix exploited by the unitary root-MUSIC algorithm [6], the special real-valued matrix can be defined by

$$\hat{\mathbf{C}}_s = \mathrm{Re}\{\mathbf{Q}_M^H\hat{\mathbf{R}}_s\mathbf{Q}_M\} \tag{35}$$

where $\hat{\mathbf{R}}_s$ denotes the estimate of the spatial smoothing covariance matrix.

4.2. Summary

Let $\mathbf{K}_{s1}$ and $\mathbf{K}_{s2}$ [4] be the real and imaginary parts of $\mathbf{Q}_{M-1}^H\mathbf{J}_s\mathbf{Q}_M$, as follows:

$$\mathbf{K}_{s1} = \mathrm{Re}\{\mathbf{Q}_{M-1}^H\mathbf{J}_s\mathbf{Q}_M\}$$

and

$$\mathbf{K}_{s2} = \mathrm{Im}\{\mathbf{Q}_{M-1}^H\mathbf{J}_s\mathbf{Q}_M\}.$$

where $\mathbf{J}_s$ is the special matrix $[\mathbf{0}_{(M-1)\times1}, \mathbf{I}_{M-1}]$. For coherent sources, we can summarize the procedure of CU-ESPRIT in the following.

Algorithm 2.

Step 1. Form the observation vector of the virtual subarrays.
Step 2. Compute the spatial smoothing covariance matrix based on Eqs. (30)–(32).
Step 3. Obtain the real-valued matrix $\hat{\mathbf{C}}_s$ by Eq. (35).
Step 4. Find the signal subspace $\mathbf{E}_s$ by taking the EVD of the matrix $\hat{\mathbf{C}}_s$.
Step 5. Compute $\mathbf{\Psi}$ as the solution to the matrix equation $(\mathbf{K}_{s1}\mathbf{E}_s)\mathbf{\Psi} = (\mathbf{K}_{s2}\mathbf{E}_s)$.
Step 6. Compute $\omega_i, i = 1, \ldots, d$ as the eigenvalues of the $d \times d$ real-valued matrix $\mathbf{\Psi}$.
Step 7. Estimate DOAs of SOIs according to (29).

5. Performance analysis

5.1. Number of estimated signals

Compared with ESPRIT, unitary ESPRIT, and NC unitary ESPRIT, CU-ESPRIT has the virtual array with $2M-1$ virtual array elements, which can estimate the same $2M-2$ uncorrelated sources as NC unitary ESPRIT, NOT confined to the element number M of the factual array. For uncorrelated signals or coherent signals, the number of estimated signals of different algorithms can be displayed in Table 1.

From Table 1, CU-ESPRIT can estimate coherent signals for virtual subarray techniques, furthermore this approach can separate up to $M-1$ coherent sources compared with NC unitary ESPRIT.

5.2. Elapsed CPU time

We should use the flop counts. This can also account for the difference in complex-valued processing versus real-valued processing. But with the use of LAPACK in Matlab, it is more appropriate to use TIC and TOC to count the elapsed CPU time, instead of FLOPS function. Then, we chose ThinkPad R61 as a convenient platform, which has a modest CPU (1.8 GHz Intel T7100) and a moderate memory space (512 MB RAM) for data processing.

Assume a ULA with five omnidirectional sensors, and the number of snapshots is 10. For simplicity, we do not consider the step of the residual phase estimation by MUSIC or ESPRIT. When we can compute elapsed CPU times with 100 000 repeating runs for ESPRIT, NC unitary ESPRIT, and CU-ESPRIT. So the elapsed CPU time of different algorithms for uncorrelated signals or coherent signals can be displayed in Tables 2 and 3. For uncorrelated sources, CU-ESPRIT has the virtual centro-symmetric array with $2M-1$ virtual elements, while CU-ESPRIT has the virtual subarrays with M virtual antennas for coherent sources. From these tables, the proposed algorithm has lower computational complexity than NC unitary ESPRIT with $2M$ virtual antennas. But considering the complexity of the residual phase estimation, CU-ESPRIT and NC unitary ESPRIT have similar computational complexities for uncorrelated case. Noted that we can also estimate coherent sources with standard ESPRIT if we combine it with spatial smoothing, as for the other algorithms.

Table 1
Number of estimated signals of different algorithms.

	Uncorrelated signals	Coherent signals
ESPRIT	$M-1$	–
Unitary ESPRIT	$M-1$	$\lfloor \frac{2}{3}M \rfloor$
NC unitary ESPRIT	$2M-2$	$\lfloor \frac{2}{3}M \rfloor$
CU-ESPRIT	$2M-2$	$M-1$

Table 2
Elapsed CPU time of different algorithms with two signals.

	Uncorrelated signals	Coherent signals
ESPRIT	2.625 s	–
NC unitary ESPRIT	6.687 s	13.172 s
CU-ESPRIT	4.579 s	3.484 s

Table 3
Elapsed CPU time of different algorithms with three signals.

	Uncorrelated signals	Coherent signals
ESPRIT	2.578 s	–
NC unitary ESPRIT	7.031 s	12.219 s
CU-ESPRIT	4.766 s	3.703 s

6. Simulation

In this section, we present some simulation results to show the behavior of CU-ESPRIT algorithm, compared with classical ESPRIT and NC unitary ESPRIT. Assume a ULA with five omnidirectional sensors spaced by a half wavelength of the coming signals and employ MASK modulated sources for simulation.

6.1. The effect of number of snapshots

In the first simulation, the root-mean-square-error (RMSE) of the CU-ESPRIT algorithm is affected by the number of snapshots with 1000 independent runs for uncorrelated sources. When the signal-to-noise ratio (SNR) is 10 dB, two uncorrelated MASK signals arrive from -35° and -15°. These methods can separate uncorrelated signals, and the CU-ESPRIT algorithm has a better performance than the NC unitary ESPRIT and the ESPRIT with the number of snapshots increasing. The results for the CU-ESPRIT, the NC unitary ESPRIT and the ESPRIT versus the number of snapshots for uncorrelated signals are plotted in Fig. 2.

In the second simulation, the RMSE of the CU-ESPRIT algorithm is affected by the number of snapshots with 1000 independent runs for coherent real sources. In Fig. 3, two coherent MASK signals arrive from -35° and -15°, the number of subarrays is four, and the SNR is 10 dB. With the number of snapshots increasing, the CU-ESPRIT and the NC unitary ESPRIT can separate coherent signals by means of spatial smoothing techniques.

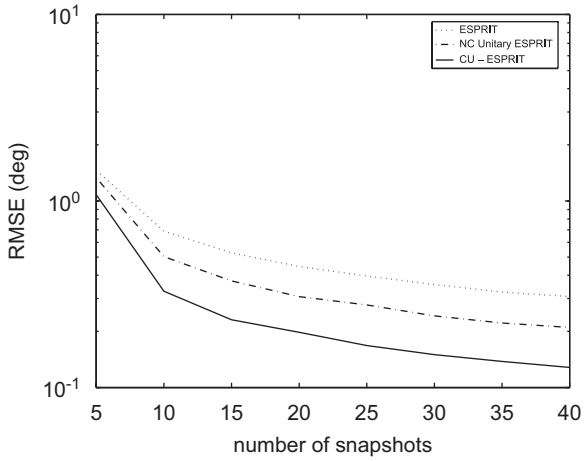

Fig. 2. RMSE versus number of snapshots for environment containing two uncorrelated MASK signals with -35° and -15° DOA (SNR = 10 dB).

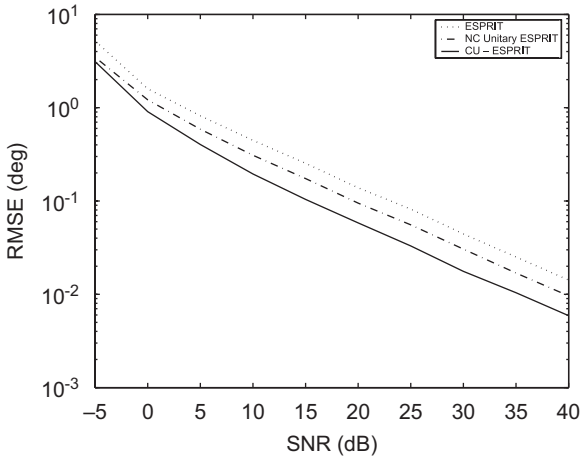

Fig. 4. RMSE versus SNR for environment containing two uncorrelated MASK signals with -35° and -15° DOA (snapshot = 20).

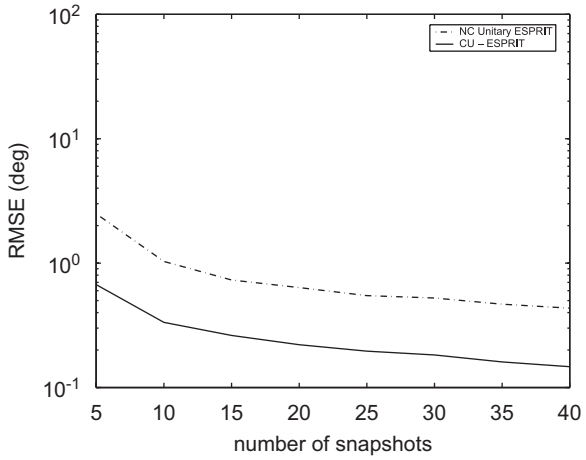

Fig. 3. RMSE versus number of snapshots for environment containing two coherent MASK signals with -35° and -15° DOA (SNR = 10 dB).

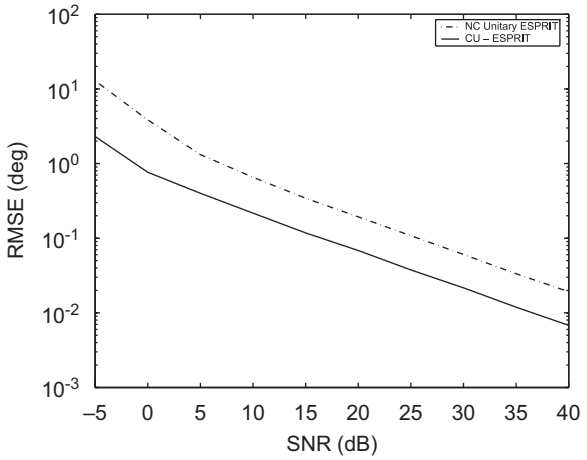

Fig. 5. RMSE versus SNR for environment containing two coherent MASK signals with -35° and -15° DOA (snapshot = 20).

From Figs. 2 and 3, the CU-ESPRIT has a better resolution than the NC unitary ESPRIT for uncorrelated or coherent signals. Note that the number of snapshots is 20 in the following simulation experiments.

6.2. The effect of SNR

In the third simulation, the performance of the CU-ESPRIT algorithm is quantified by the RMSE with 1000 independent runs for uncorrelated real sources. Two uncorrelated MASK signals arrive from -35° and -15°. As the SNR increases, these methods can separate uncorrelated signals, and the CU-ESPRIT has a better performance than the NC unitary ESPRIT and the ESPRIT. The results for the CU-ESPRIT, the NC unitary ESPRIT and the ESPRIT versus the SNR for uncorrelated signals are plotted in Fig. 4.

In the fourth simulation, the RMSE of the CU-ESPRIT algorithm is affected by the SNR with 1000 independent runs, when two coherent MASK signals arrive from -35° and -15° DOA and the number of subarrays is four. The CU-ESPRIT and the NC unitary ESPRIT can estimate coherent signals, but the CU-ESPRIT has a better resolution than the NC unitary ESPRIT. The results for the CU-ESPRIT, the NC unitary ESPRIT versus the SNR for coherent real sources are plotted in Fig. 5.

Compared with the NC unitary ESPRIT, the CU-ESPRIT has lower RMSE values for uncorrelated or coherent real sources in Figs. 4 and 5 when the SNR increases.

6.3. The effect of angular separation

In the fifth simulation, the RMSE of the CU-ESPRIT algorithm is affected by the angular separation with 1000 independent runs for two uncorrelated real sources from

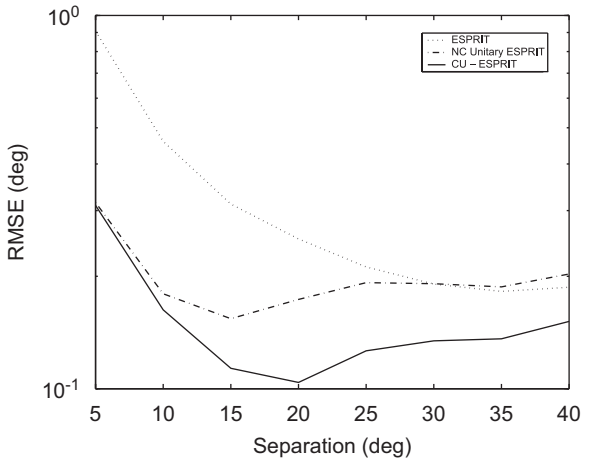

Fig. 6. RMSE versus angular separation for environment containing two uncorrelated MASK signals ($\theta_1 = -15^\circ$, snapshot = 20, SNR = 15 dB).

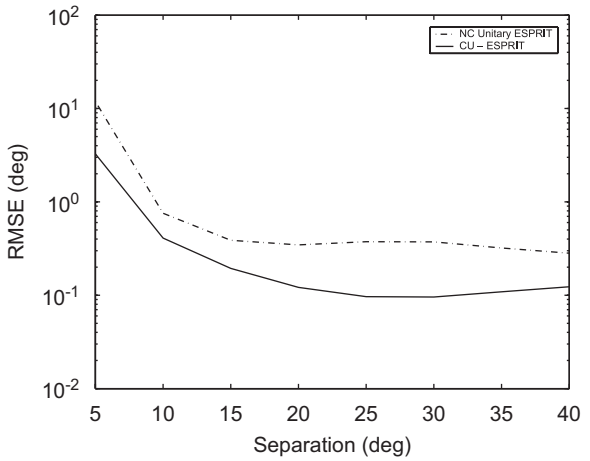

Fig. 7. RMSE versus angular separation for environment containing two coherent MASK signals ($\theta_1 = -15^\circ$, snapshot = 20, SNR = 15 dB).

$\theta_1 = -15^\circ$ and $\theta_2 = (-15 + sep)^\circ$ when the SNR is 15 dB. When the angular separation is from 5° to 40°, the CU-ESPRIT has a better performance than the NC unitary ESPRIT and the ESPRIT. The results for the CU-ESPRIT, the NC unitary ESPRIT and the ESPRIT versus the angular separation for uncorrelated signals are plotted in Fig. 6.

In the sixth simulation, the RMSE of the CU-ESPRIT algorithm is affected by the angular separation with 1000 independent runs for coherent real sources from $\theta_1 = -15^\circ$ and $\theta_2 = (-15 + sep)^\circ$, when the SNR is 15 dB and the number of subarrays is four. When the angular separation is from 5° to 40°, the CU-ESPRIT has a better performance than the NC unitary ESPRIT in Fig. 7.

In Figs. 6 and 7, the CU-ESPRIT has a better performance than the NC unitary ESPRIT for uncorrelated or coherent sources with the angular separation varying. Note that the CU-ESPRIT and the NC unitary ESPRIT have some oscillations in relative values. For a separation of 15° the second source is at 0°, i.e., the broad side of the array where the resolution is best, and for bigger separations the second source comes closer to the bore side where the resolution gets worse.

6.4. The effect of number of signals

In the seventh simulation, the RMSE of the CU-ESPRIT method is affected by the number of uncorrelated real sources. When the SNR is 20 dB, $\theta_1 = 0^\circ$, angular separation $= 15^\circ$. When eight sources are used, they arrive from -45°, -30°, -15°, 0°, 15°, 30°, 45°, and 60° DOA. With the number of signals rising, the RMSEs of the CU-ESPRIT and the NC unitary ESPRIT are getting larger, the CU-ESPRIT has a better resolution than the NC unitary ESPRIT. The results of 1000 trial runs for these two methods versus the number of signals are plotted in Fig. 8.

In the eighth simulation, the maximum number of estimated coherent real sources is tested by

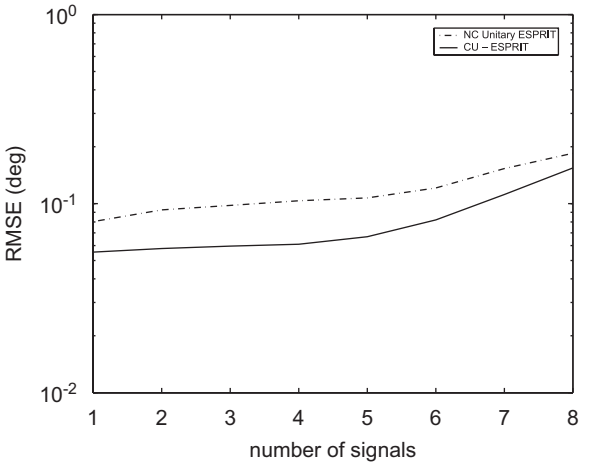

Fig. 8. RMSE versus number of uncorrelated MASK signals ($\theta_1 = 0^\circ$, angular separation = 15°, snapshot = 20, SNR = 15 dB).

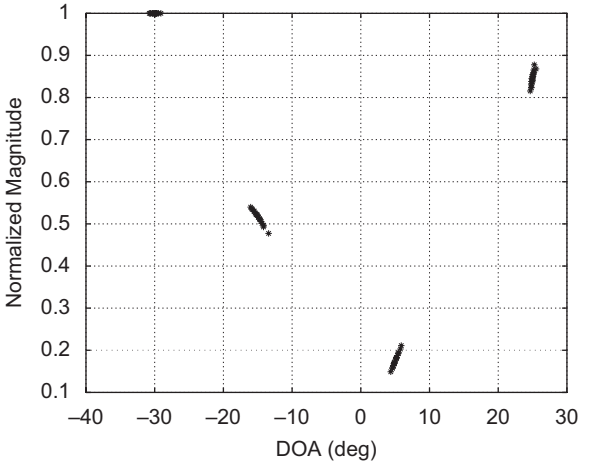

Fig. 9. Spatial spectra for environment containing four coherent MASK signals with -30°, -15°, 5°, and 25° DOA. With the CU-ESPRIT (star).

20 independent DOA estimates. When the SNR is 20dB, four coherent MASK signals arrive from -30°, -15°, 5°, and 25° DOA. From Fig. 9, the CU-ESPRIT can estimate four coherent signals. In other words, this proposed method can separate as many as $M-1$ coherent sources.

6.5. The effect of residual delay

In the last two simulations, the RMSE of the CU-ESPRIT method is affected by the residual delay from the phase compensation with 1000 independent trial runs where T_s is the symbol period. From Fig. 10, two MASK signals arrive from -30° and -15° DOA when the SNR is 20 dB.When two MASK signals are coherent,the number of subarrays is four. For uncorrelated signals or coherent signals, the residual delay has a significant effect on the performance of the proposed method. In order to evaluate this algorithm under some residual delay further, the Cramer–Rao bound (CRB) [14,15] is used. In Fig. 11, two uncorrelated MASK signals arrive from -30° and -15° DOA. When the residual delay varies in order, the results of 1000 trial runs for the RMSE versus the SNR are given with reference to the CRB. This shows that it is realistic to assume that real-valued sources can be achieved when the residual delays are very small. Therefore, it is a good choice to minimize the residual delay by selecting a high-resolutioned phase estimation and compensation scheme.

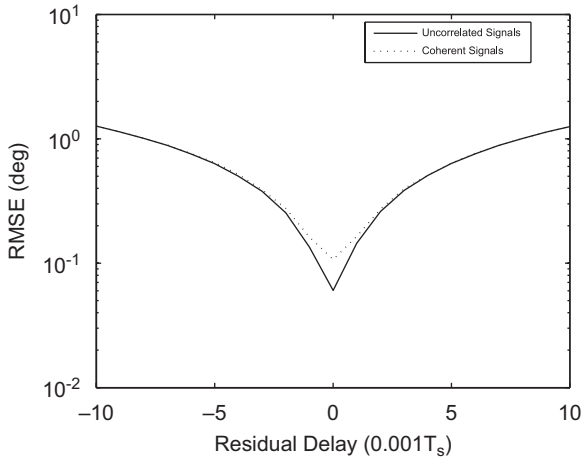

Fig. 10. RMSE versus residual delay for environment containing two MASK signals with -30°, and -15° DOA (snapshot = 20, SNR = 20 dB).

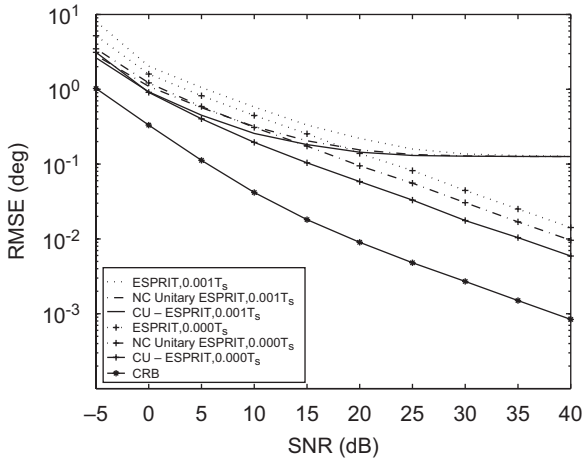

Fig. 11. RMSE versus SNR for environment containing two uncorrelated MASK signals with -30°, and -15° DOA (residual delays = $\{0.000T_s, 0.001T_s\}$, snapshot = 20).

7. Conclusion

In this paper, we present a new unitary ESPRIT algorithm for real-valued sources, by designing a virtual centro-symmetric array for uncorrelated signals and dividing it into the virtual subarrays for highly correlated or coherent signals. This approach has a higher resolution and lower computational complexity than the NC unitary ESPRIT for uncorrelated or coherent signals. Most importantly, this method can estimate up to $M-1$ coherent sources for an M-elemented array benefited from the division of M overlapping subarrays.

We have also conducted computer experiments to show the superiority of our method over the NC unitary ESPRIT and the conventional ESPRIT in aspects of number of snapshots, SNR, angular separation and number of signals. Simulation results are consistent with our analysis on the real-valued property of the sources and the higher number of separable coherent sources.

References

[1] K.C. Huarng, C.C. Yeh, A unitary transformation method for angle of arrival estimation, IEEE Trans. Acoust. Speech Signal Process. 39 (April 1991) 975–977.
[2] M.D. Zoltowski, G.M. Kautz, S.D. Silverstein, Beamspace root-MUSIC, IEEE Trans. Signal Process. 41 (January 1993) 344–364.
[3] M. Haardt, J.A. Nossek, Unitary ESPRIT: how to obtain increased estimation accuracy with a reduced computational burden, IEEE Trans. Signal Process. 43 (May 1995) 1232–1242.
[4] M.D. Zoltowski, M. Haardt, C.P. Mathews, Closed-form 2-D angle estimation with rectangular arrays in element space or beamspace via unitary ESPRIT, IEEE Trans. Signal Process. 44 (February 1996) 316–328.
[5] A.B. Gershman, M. Haardt, Improving the performance of Unitary ESPRIT via pseudo-noise resampling, IEEE Trans. Signal Process. 47 (August 1999) 2305–2308.
[6] M. Pesavento, A.B. Gershman, M. Haardt, Unitary root-MUSIC with a real-valued eigendecomposition: a theoretical and experimental performance study, IEEE Trans. Signal Process. 48 (May 2000) 1306–1314.
[7] N. Tayem, H.M. Kwon, Conjugate ESPRIT, IEEE Trans. Antennas Propag. 52 (October 2004) 2618–2624.
[8] M. Haardt, F. Römer, Enhancements of unitary ESPRIT for non-circular sources, in: Proceedings of the IEEE ICASSP, Montreal, Canada, vol. II, May 2004, pp. 101–104.
[9] F. Römer, M. Haardt, Efficient 1-D and 2-D DoA Estimation for non-circular sources with hexagonal shaped ESPAR arrays, in: Proceedings of the IEEE ICASSP, Toulouse, France, vol. IV, May 2006, pp. 881–884.
[10] T.J. Shan, M. Wax, T. Kailath, On spatial smoothing for direction-of-arrival estimation of coherent signals, IEEE Trans. Acoust. Speech Signal Process. 33 (August 1985) 806–811.
[11] R.T. Williams, S. Prasad, A.K. Mahalanabis, L.H. Sibul, An improved spatial smoothing technique for bearing estimation in a multipath environment, IEEE Trans. Acoust. Speech Signal Process. 36 (April 1988) 425–432.

[12] S.U. Pillai, B.H. Kwon, Forward/backward spatial smoothing techniques for coherent signal identification, IEEE Trans. Acoust. Speech Signal Process. 37 (January 1989) 8–15.
[13] R. Roy, T. Kailath, ESPRIT-estimation of signal parameters via rotational invariance techniques, IEEE Trans. Acoust. Speech Signal Process. 37 (July 1989) 984–995.
[14] P. Stoica, A. Nehorai, MUSIC, maximum likelihood, and Crámer–Rao bound, IEEE Trans. Acoust. Speech Signal Process. 37 (May 1989) 720–741.
[15] J. Delmas, H. Abeida, Stochastic Crámer–Rao bound for noncircular signals with application to DoA estimation, IEEE Trans. Signal Process. 52 (November 2004) 3192–3199.